Transmission Loss and Dynamic Response of Hierarchical Membrane-Type Acoustic Metamaterials

William T. Edwards[1], Chia-Ming Chang[2], Geoffrey McKnight[2], Adam Sorensen[2], Steven R. Nutt[1*]

[1]M.C. Gill Composites Center, Department of Chemical Engineering and Materials Science, University of Southern California, 3651 Watt Way VHE-602, Los Angeles, CA 90089-0241, USA

[2] HRL Laboratories, 3011 Malibu Canyon Road, Malibu, CA 90265

* E-mail: nutt@usc.edu

Abstract: A deployment-scale array of locally resonant membrane-type acoustic metamaterials (MAMs) is fabricated. The acoustic performance of the array is measured in a transmission loss chamber, and a complex interaction between the individual cell and the array length scales is shown to exist. Transmission behavior of both the membrane and the array are independently studied using analytical models, and a method for estimating transmission loss through the structure that combines vibroacoustic predictions from both length scales is presented and shown to agree with measurements. Degradation of transmission loss performance often associated with scaling individual MAM cells into arrays is explained using analytical tools and verified using laser vibrometry. A novel design for hierarchical locally resonant acoustic metamaterials is introduced, and experimental and analytical data confirm this approach offers an effective strategy for minimizing or eliminating the efficiency losses associated with scaling MAM structures. [DOI: 10.1115/1.4045789]

Keywords: dynamics, materials in vibration and acoustics, modal analysis, noise control

1. INTRODUCTION

Designing acoustic barriers that reject low-frequency noise transmission has been a particularly challenging task for materials scientists and acousticians. Typical approaches for reducing

Please cite the article as: WT Edwards and S Nutt **“Transmission Loss and Dynamic Response of Hierarchical Acoustic Metamaterials”,** Journal of Vibration and Acoustics (2019) DOI: 10.1115/1.4045789

sound transmission through an acoustic barrier generally rely on increasing the thickness or density of the barrier in question. Transmission efficiency through these structures can be predicted using the acoustic mass law, but experimental data indicate that many structures underperform this benchmark [1]. Further, the acoustic mass law indicates that for such strategies to be effective in the low-frequency regime (20–2000 Hz), a significant addition of mass is required. For weight-critical applications, this additional mass may be untenable, and alternative solutions are demanded.

To address the need for a slim, weight-efficient acoustic barrier effective at low frequencies, membrane-type acoustic metamaterials (MAMs) were conceived [2]. Experimental and finite element modelling demonstrated that membrane-type acoustic metamaterials significantly outperform the acoustic mass law in certain frequency ranges [3]. Comprising one or more masses bonded to a pretensioned membrane, MAMs exhibit a characteristic transmission profile that can be tuned with respect to frequency by adjusting the size of the masses or changing the tension in the membrane [4]. The influences of membrane geometry and mass location have been measured using a transmission loss tube and predicted using finite element models [5]. While MAMs can be entirely passive structures, work has been done to explore the active frequency response tuning and energy harvesting using a variety of approaches [6–8].

Structures similar to MAMs have been investigated for use in duct silencing where a tensioned membrane (with no mass bonded to it) replaced a portion of the duct wall to reflect gracing incident noise [9]. In such structures, acoustic propagation is directed primarily parallel to the surface of the membrane, whereas MAMs are typically tuned for normally incident acoustic propagation. Demonstration of duct-membrane systems both with and without sealed

Please cite the article as: WT Edwards and S Nutt **“Transmission Loss and Dynamic Response of Hierarchical Acoustic Metamaterials”,** Journal of Vibration and Acoustics (2019) DOI: 10.1115/1.4045789

backing cavities provide acousticians with a better understanding of how membrane geometry and tension influence the acoustic performance of such structures [10,11].

While finite element tools have been shown to accurately predict the acoustic performance of MAMs, their implementation is not well suited for some design and optimization challenges. Parametric analysis of one or more geometric variables (e.g., size, shape, location, or the number of masses) would be particularly inefficient using finite element methods, as it would require successive remeshing of the bodies involved. Alternatively, analytical methods can be easily implemented, efficiently used, and seamlessly integrated with automated design optimization tools. This has driven the development of several analytical tools for the prediction of sound transmission through MAMs with a variety of geometries. Chen et al. developed coupled vibroacoustic analytical models for both circular and Cartesian membranes under tension with fixed boundaries, using a point-matching approach to capture the influence of the attached mass [12]. Langfeldt et al. simplified the numerical implementation of this model by using dimensionless parameters to compose a linear eigenvalue problem and decoupling the membrane from the surrounding air to avoid costly numerical integration [13]. Both models assume that the stiffness of the membrane contributes no restorative force during MAM excitation and deformation.

Other analytical models were developed to capture the influence of bending stiffness on MAM performance. An acoustically coupled analytical model describing membrane motion according to pre-tensioned plate-like dynamic equations was developed but was limited to MAMs with clamped boundaries and required any masses to be placed symmetrically about both the midplanes of the surface of the membrane [14]. Efforts to develop a similar model that considers bending effects, relaxes symmetry and boundary condition limitations, and integrates the numerical efficiency of the model presented in [13] culminated in analytical tools that accommodate any combination of simply supported and clamped boundaries and allow for an arbitrary number of masses with no symmetry requirements [15].

Efforts to scale MAMs beyond a single cell have investigated arranging several membranes in series and in parallel. Arranging MAMs in series—such that acoustic energy is transmitted sequentially through each membrane structure—has been shown to increase transmission loss, and independent tuning of each MAM allows designers more control over the spectral response of the system [16]. Initial investigation into scaling MAMs in the in-plane direction has been conducted by the same authors by creating an array of several membranes, creating parallel transmission paths for acoustic energy. Small samples have been fabricated and tested in a transmission loss tube with results indicating that even incremental scaling (from one membrane to four) results in the decay of favorable transmission properties [17]. Modeling efforts describing multi-celled arrays of MAMs in a single panel have resulted in an analytical model that produces more realistic predictions for the transmission loss through arrays of membranes that can each be independently tuned [18]. This model, however, assumes that each edge of each membrane cell is fixed (i.e., the membrane support grid is rigid).

Efforts to deploy increasingly larger arrays of membrane cells have been thwarted by similar decay of the theoretical transmission loss performance. It has been primarily thought that this performance decay is linked to the motion of the array frame (the substrate on which the membranes are bonded), where this motion violates the assumption that individual membrane resonators have fixed boundaries. To reduce the magnitude of frame motion—and thereby mitigate this issue, stiffer materials have been investigated for use as a substrate by the authors. Preliminary results have suggested this is not a comprehensive solution.

Some efforts have been made to capture the influence of array compliance in multi-celled MAM arrays using numerical and analytical techniques. Langfeldt et al. used numerical techniques to begin exploring the importance of considering grid compliance when estimating transmission loss for very low frequencies [18]. Subsequently, the relationship between MAM boundary compliance and transmission loss was further explored when an analytical model was developed that accommodates elastic MAM cell edges [19].

An alternative strategy for addressing performance knockdowns associated with membrane array scaling is presented here. We suggest that a hierarchical approach can be taken: the array of MAMs can be considered analogous to an individual membrane cell where the bending stiffness of the array plays the same role as the tension in the membrane cell and a mass of appropriate size is bonded to the array. In hierarchical structures, the material is organized at different length scales, and structural elements comprise one or multiple sub-levels of structural organization. Such hierarchically organized materials occur naturally in tooth enamel and spider silk, for example, and it is their hierarchical organization that results in emergent mechanical properties [20,21]. Prior to this work, the principles of hierarchical design have been successfully applied to a variety of acoustic metamaterials to broaden the frequency ranges in which desirable behavior occurs. For example, Zhang and To presented a hierarchical phononic crystal that achieved bandgaps in order of magnitude larger than those exhibited in conventional structure [22]. A variety of other hierarchical metamaterials have been studied [23–25], but to the authors' knowledge, this work represents the first time such principles have been applied to membrane-type acoustic metamaterials.

To demonstrate the effectiveness of a hierarchical design approach in controlling the dynamic response of an array of MAMs, we detail the first fabrication and experimental characterization of a deployment-scale, hierarchical MAM. The primary contributions of this work are (1) to explain the decay of transmission loss performance associated with scaling from one MAM to an array of MAMs, (2) to demonstrate a design solution in the form of a novel hierarchical acoustic metamaterial structure, and (3) to explore and explain the behavior of such a hierarchical membrane structure. These contributions are enabled by the application and verification of analytical modeling tools that enable uncovering of the physical mechanism by which the transmission loss profile of an array of membranes differs from that of an individual, identically tuned membrane. The modeling tools developed for this purpose also provide predictive tools to the acoustician for use when designing hierarchical MAMs.

Section 2 contains (a) details regarding the fabrication of a hierarchical MAM array, (b) the methods used to measure transmission loss and modal response, and (c) details about the implementation of analytical models describing each length scale of the structure. In Sec. 3, experimental and analytical data explaining the transmission loss performance characteristics of hierarchical MAMs are presented. Further, the influences of changing the size of the mass bonded to the array and to each membrane are demonstrated and discussed. Finally, a summary of findings is shared, and the implications thereof are explored.

2 METHODS

2.1 Fabrication of Membrane Array. An array of 36 MAM cells was fabricated by first milling a six-by-six grid of 4×10^{-2} m by 4×10^{-2} m square holes through a 0.251 m by 0.251 m by 7.5×10^{-3} m thick plate of aluminum. The holes were located such that each of the four exterior edges of the plate was $3 \times 10-3$ m wide, and the material remaining between each hole was 1×10^{-3} m across. After machining, the surface of the plate was covered with an epoxy adhesive over which a $7.62 \times 10-5$ m thick film of polyethylene terephthalate (PET) was draped. The assembly was placed into an oven and warmed to 120 °C during which time the PET was bonded to the aluminum plate. After the epoxy adhesive cured, the assembly was removed from the oven and allowed to cool, during which time dissimilar thermal expansion properties introduced a residual tensile stress in each of the membrane cells.

Please cite the article as: WT Edwards and S Nutt **"Transmission Loss and Dynamic Response of Hierarchical Acoustic Metamaterials",** Journal of Vibration and Acoustics (2019) DOI: 10.1115/1.4045789

In the center of each prestressed membrane cell, an annular inertial inclusion of interior diameter 9.53×10^{-3} m and exterior diameter $1.59 \times 10{-}2$ m was bonded. Investigations using inclusions of thickness $5.1 \times 10{-}4$ m (mass $1.6 \times 10{-}4$ kg) as well as thickness 1.1×10^{-3} m (mass $3.20 \times 10{-}4$ kg) were conducted; in each case, a spray adhesive was used to bond the inclusions to the membrane cells. Figure 1 shows a photograph of the completed MAM array. The system's two levels of hierarchy are depicted schematically in Figure 2, where the entire array structure and large centrally bonded mass (not pictured in Figure 1) constitute one level of the hierarchy, and an individual membrane cell with corresponding inclusion constitutes another.

2.2 Transmission Loss Testing and Modal Analysis. A small-scale, two-chamber transmission loss test facility, constructed in accordance with ASTM 2249-02 [26], was used to measure random-incidence transmission loss through the membrane metamaterial array with various and mass loading conditions (on both the individual membrane cells and the array structure). The facility comprised a reverberant chamber (15 m3) and an anechoic chamber (12 m^3), separated by a square (0.241 m× 0.241 m) orifice used to hold the test panel. To ensure clamped boundary conditions on the membrane array, the test panels were mounted covering

Please cite the article as: WT Edwards and S Nutt **"Transmission Loss and Dynamic Response of Hierarchical Acoustic Metamaterials",** Journal of Vibration and Acoustics (2019) DOI: 10.1115/1.4045789

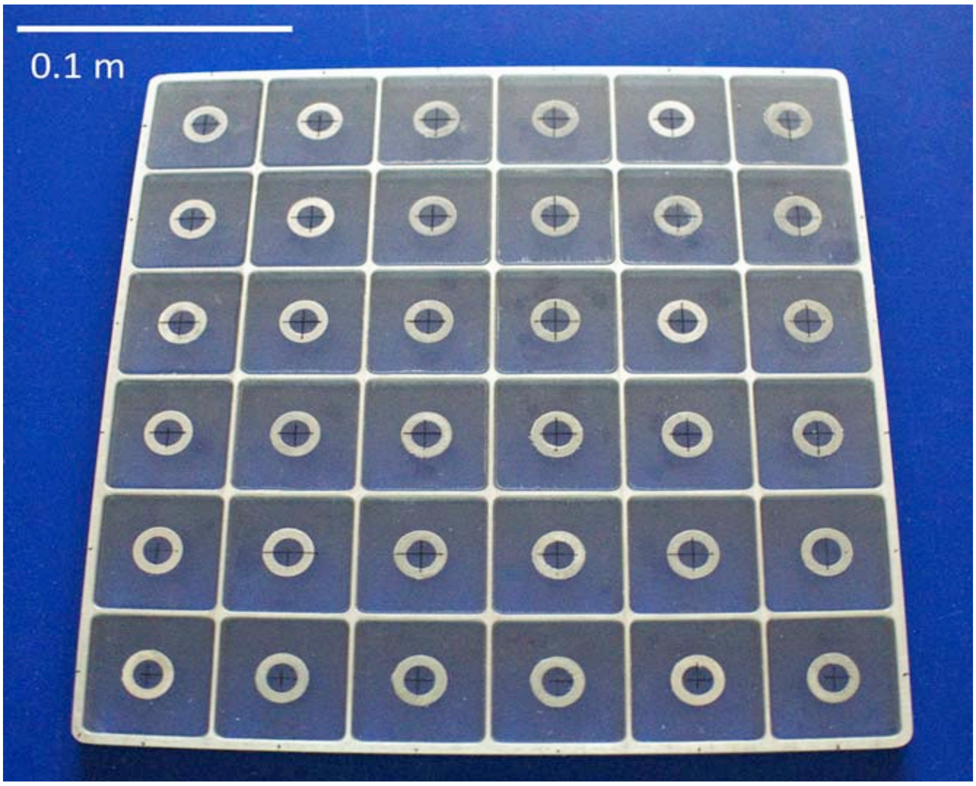

Figure 1. Photograph of completed hierarchical membrane-type metamaterial acoustic barrier

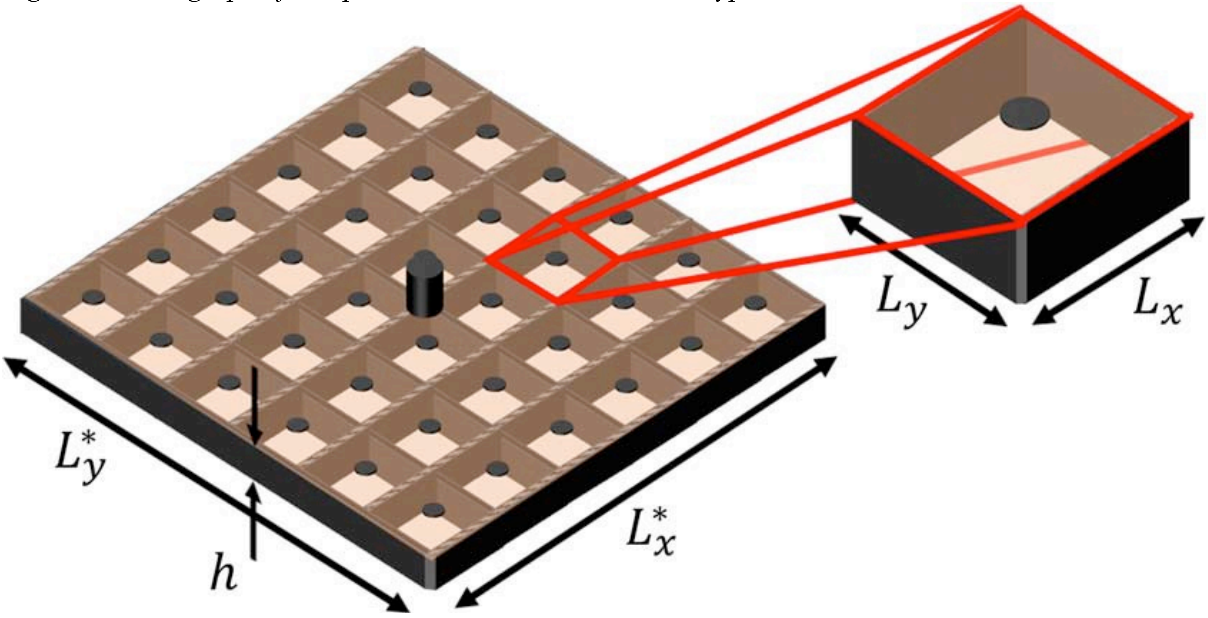

Figure 2. Schematic representing two tiers of design hierarchy: array level and individual cell level

the orifice using an aluminum frame and tightly bolted at 16 equally spaced locations around the perimeter of the sample as shown in Fig. 3. Fasteners were tightened with a torque-controlled hand drill to achieve maximally consistent mounting conditions.

Please cite the article as: WT Edwards and S Nutt **"Transmission Loss and Dynamic Response of Hierarchical Acoustic Metamaterials",** Journal of Vibration and Acoustics (2019) DOI: 10.1115/1.4045789

An acoustic signal was generated in the reverberant chamber, where nine nonparallel, reflective walls produced a diffuse sound field measured using a rotating boom sound pressure level microphone to determine a spatially averaged sound pressure level intensity. In the anechoic chamber, the transmitted acoustic energy was measured using an intensity probe on

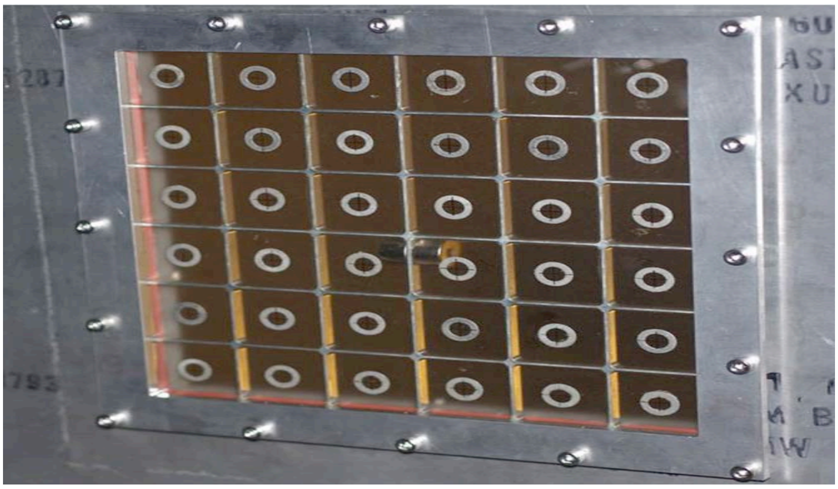

Fig. 3 Metamaterial sample mounted in the transmission loss chamber with clamped boundaries

a motorized gantry located 0.17 m away from the test panel. Measurements were collected at equally spaced locations to determine an average transmission loss through the whole membrane array. The frequency range of the noise source was 100 Hz–6.4 kHz and source-side pressure levels were maintained at between 90 and 95 dB for all tests. Previous work determined the cutoff frequency of the diffuse field—due to the geometry of the reverberant chamber—to be 315 Hz [27].

For several samples, the out-of-plane motion of the array during vibration was determined using a laser vibrometer (Ometron VH300+ Laser Doppler Vibrometer Type 8329) to measure the motion of 85 discrete points within the domain of the aluminum array. Vibrometry measurements were collected at each midpoint along each edge and each corner of each membrane cell, excluding cell edges and corners on the boundary of the array. For each measurement, sound pressure levels in the reverberant room were also recorded. The frequency range of the noise source was 100 Hz–6.4 kHz. For each of the 85 points measured, auto- and crosscorrelations were used to calculate the H2 transfer function relating the motion of the array (vibrometer signal) to the acoustic excitation (sound pressure signal) as a function of frequency. At frequencies where coherence between these signals was high for many of the measured points, the data were used to determine natural frequencies and recover an estimate of their corresponding modal responses.

2.3 Analytical Model. To further confirm and study the transmission properties of hierarchical MAMs, analytical models were implemented, capturing the behavior of individual membrane cells, the entire array, and the two length scales in concert (referred to going forward as the compound system). Below, we describe in detail the mathematics used to model each length scale of the hierarchical MAM array structure. In Sec. 2.3.1, we present relevant details of the fourth-order model used to approximate the vibration of the array, described as a Kirchhoff–Love plate with homogenized stiffness and mass properties and clamped boundaries. In Section 2.3.2, we highlight the parallel mathematical framework used to describe the motion of individual membrane cells, described according to second-order dynamics, and define analogous terms and parameters. Finally, we present an approach for predicting the transmission loss through the compound structure using both models in conjunction.

2.3.1 Modeling Array Behavior: Plate-Like Dynamics. Using the model presented in Ref. [15], we approximate the array structure as a monolithic isotropic plate of dimensions L_x^* and L_y^*, homogenized surface mass density m_A', and homogenized effective bending stiffness T*. A rigid inertial inclusion of mass M_A is bonded to the array, its center of mass is located at coordinates $[x_{CM}^*, y_{CM}^*]$, and its rotational moments of inertia about the $\vec{y}^{*\prime}$ and $\vec{x}^{*\prime}$ axes are given as J_{x^*} and J_{y^*} respectively, where the coordinate frame $\{\vec{x}^{*\prime}, \vec{y}^{*\prime}, \vec{z}^{*}\}$ is defined such that its origin is located at the center of mass of the inertial inclusion. As shown in Figure 4, the origin of the coordinate frame $\{\vec{x}^{*}, \vec{y}^{*}, \vec{z}^{*}\}$ is located at one corner of the plate with the

Please cite the article as: WT Edwards and S Nutt **"Transmission Loss and Dynamic Response of Hierarchical Acoustic Metamaterials",** Journal of Vibration and Acoustics (2019) DOI: 10.1115/1.4045789

positive x *-axis and y *-axis oriented along edges of the plate and the z *-axis orthogonal to the plate surface with the positive direction defined in accordance with the right-hand rule. The out-of-plane displacement of the plate is given by $w^*(x^*, y^*, t)$ and its motion is governed by Kirchhoff–Love plate dynamics

$$m_A' \frac{\partial^2}{\partial t^2} w^*(x^*, y^*, t) + T^* \nabla^2 \nabla^2 w^*(x^*, y^*, t) = P(x^*, y^*, t) + f'_A(x^*, y^*, t) \tag{1}$$

where $\nabla^2 = \partial^2/\partial x^2 + \partial^2/\partial y^2$ is the Laplace operator in Cartesian coordinates, $P(x^*, y^*, t)$ is the acoustic pressure acting on the array, and f'_A is the coupling force resulting from inertial inclusions mounted to the array. Assuming harmonic time dependence and normally incident incoming acoustic excitation, we can write

$$w^*(x^*, y^*, t) = \hat{w}^*(x^*, y^*)e^{i\omega t} \tag{2}$$

$$P(x^*, y^*, t) = \hat{P}(x^*, y^*)e^{i\omega t} \tag{3}$$

$$f'(x^*, y^*, t) = \hat{f}'(x^*, y^*)e^{i\omega t} \tag{4}$$

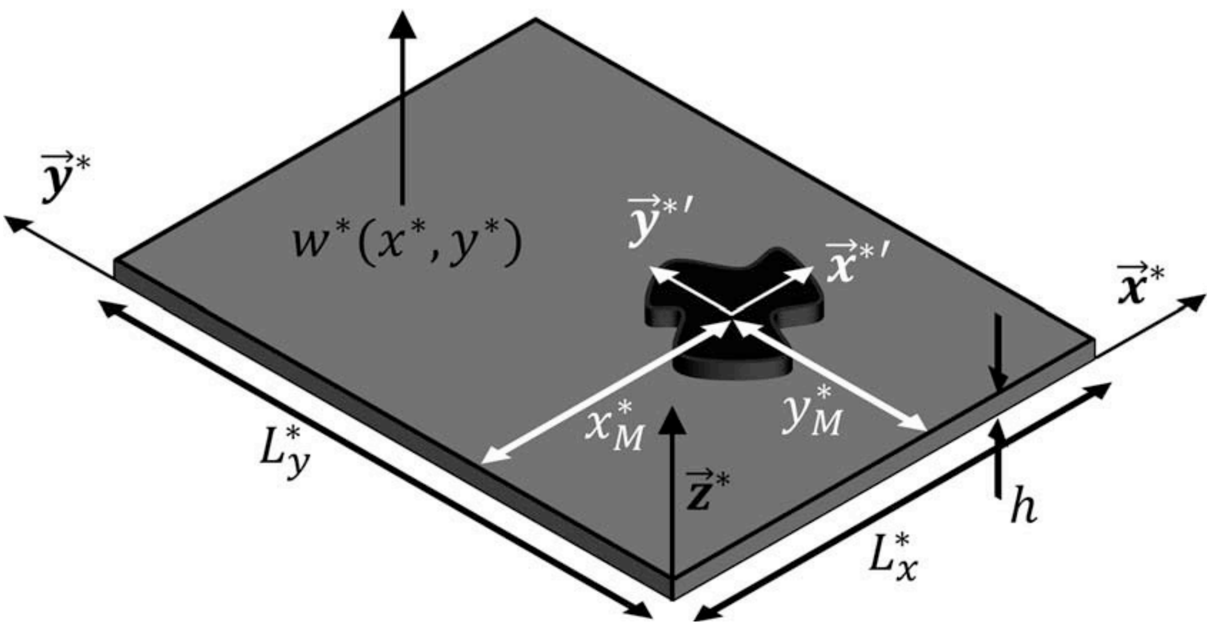

Fig. 4 Definition of geometric and mathematical variables for modeling array behavior

For the sake of brevity and clarity, the time dependence of the terms in Eqs. (2)–(4) is omitted from all following mathematical expressions. Dimensionless parameters are then defined according to

$$\xi^* = x^*/L_x^* \qquad \eta^* = y^*/L_y^* \qquad \zeta^* = z^*/L_x^* \qquad u^* = \widehat{w}_x^*/L_x^*$$
$$\Lambda = L_x^*/L_y^* \qquad \beta^* = \widehat{P}L_x^*/T^* \qquad k^{*2} = m'_A\omega^2 L_x^{*4}/T^* \qquad \gamma^* = \hat{f}'_A L_x^2/T^* \tag{5}$$

The dimensionless parameters given by Equation (5) simplify Equation (1) to

$$-k^{*2}u^* + \frac{\partial^4 u^*}{\partial \xi^{*4}} + 2\,\Lambda^{*2}\frac{\partial^4 u^*}{\partial \xi^{*2}\,\partial \eta^{*2}} + \Lambda^{*4}\frac{\partial^4 u^*}{\partial \eta^{*4}} = \beta^* + \gamma^* \tag{6}$$

The influence of the rigid mass is captured using a point-matching approach to approximate the coupling force that is applied over a continuous domain as a finite set of I* forces that act at discrete points within and on the boundary of the domain of the inclusion. The coupling force is expressed as

$$\gamma^* = \sum_{i=1}^{I^*} \gamma_i^* \delta\,(\xi^* - \xi_i^*)\,\delta\,(\eta^* - \eta_i^*) \tag{7}$$

where γ_i^* is the dimensionless coupling force contributed by the i^{th} collocation point and δ is the Dirac delta function. Substituting Equation (7) into Equation (6), the resulting equation is solved using a modal expansion approach, approximating the response of the system as a finite linear combination of N* eigenfunctions $\Phi^*(\xi^*, \eta^*)$ determined by the boundary conditions and geometry of the system. In this implementation, the boundaries of the array are assumed to be rigidly clamped to a support structure, resulting in boundary conditions given by

$$u^*(0,\eta^*) = u^*(\xi^*,0) = u^*\left(\xi^*, L_y^*\right) = u^*(L_x^*,\eta^*) = 0$$
$$\frac{\partial u^*(0,\eta^*)}{\partial \xi} = \frac{\partial u^*(\xi^*,0)}{\partial \eta} = \frac{\partial u^*\left(\xi^*,L_y^*\right)}{\partial \xi} = \frac{\partial u^*(L_x^*,\eta^*)}{\partial \eta} = 0 \tag{8}$$

To satisfy these boundary conditions, the eigenfunction $\Phi_{n_x n_y}^*(\xi^*,\eta^*) = \Phi_{n_x}^*(\xi^*)\Phi_{n_y}^*(\eta^*)$ is chosen such that $\Phi_n^*(\varpi) = \cosh(a_n\varpi) - \cos(a_n\varpi) - b_n(\sinh(a_n\varpi) - \sin(a_n\varpi))$ is the n^{th} mode shapes of a clamped–clamped single-span beam.

Please cite the article as: WT Edwards and S Nutt **"Transmission Loss and Dynamic Response of Hierarchical Acoustic Metamaterials",** Journal of Vibration and Acoustics (2019) DOI: 10.1115/1.4045789

The coefficients an are the solutions to

$\cos(a_n)\cosh(a_n) = 1$ (9)

and the corresponding coefficients b_n are determined according to

$$b_n = \frac{\sinh(a_n)+\sin(a_n)}{\cosh(a_n)-\cos(a_n)} \tag{10}$$

The unitless modal displacement is then approximated according to

$$u \approx \sum_{n=1}^{N^*} q_n^* \phi_n^* = \sum_{n_x=1}^{N_x^*} \sum_{n_y=1}^{N_y^*} q_{n_x n_y}^* \phi_{n_x}^*(\xi^*) \phi_{n_y}^*(\eta^*) \tag{11}$$

where $N^* = N_x^* N_y^*$ and $n = N_y^* (n_x - 1) + n_y$.

After substituting Equations (7) and (11) into Equation (6), the equations of motion can be arranged into matrix form according to

$$(\boldsymbol{C}^* - k^{*2}\boldsymbol{M}^*)\mathbf{q}^* = \beta^*\mathbf{b}^* + \mathbf{L}^*\gamma^* \tag{12}$$

where the dimensionless coupling-force vector γ^* contains entries $[\gamma_1^*, \gamma_2^*, \ldots, \gamma_{N^*}^*]^T$, the stiffness matrix $\boldsymbol{C}^* = (c_{mn}^*) \epsilon \mathbb{R}^{N^* \times N^*}$, the mass matrix $\boldsymbol{M}^* = (c_{mn}^*) \epsilon \mathbb{R}^{N^* \times N^*}$ has entries given by

$$c_{mn}^* = \begin{cases} a_n^{*4} + 2\wedge^{*2}((b_n^2 a_n^2)(2 - b_n a_n)^2) + \wedge^{*4} a_n^4 & for\ m = n \\ 0 & else \end{cases} \tag{13}$$

$$m_{mn} = \begin{cases} 1 & for\ m = n \\ 0 & else \end{cases} \tag{14}$$

and the coupling matrix $\mathbf{L}^* = (l_{mn}^*) \epsilon \mathbb{R}^{N^* \times I^*}$ and forcing vector $\mathbf{b}^* = (b_n^*) \epsilon \mathbb{R}^{N^*}$ have entries given by

$$l_{mn}^* = \phi_{n_x}^*(\xi_n^*)\, \phi_{n_y}^*(\eta_n^*) \tag{15}$$

$$b_n = \begin{cases} \frac{16 b_{n_x} b_{n_y}}{a_{n_x} a_{n_y}} & \text{for } n_x n_y \text{ odd} \\ 0 & \text{else} \end{cases} \tag{16}$$

The second set of equations is developed to describe the motion of the inertial inclusion. This set of equations is written in the coordinate frame $\{\vec{x}^{*\prime}, \vec{y}^{*\prime}, \vec{z}^{*}\}$ whose origin is located at

Please cite the article as: WT Edwards and S Nutt **"Transmission Loss and Dynamic Response of Hierarchical Acoustic Metamaterials",** Journal of Vibration and Acoustics (2019) DOI: 10.1115/1.4045789

the center of mass of the inertial inclusion mounted to the array (see Figure 4). The displacement anywhere within the domain of the rigid inclusion can be related to the position of its center of mass $u_{A,CM}$ and two terms α_{ξ^*} and α_{η^*} describing its rotation about the $x^{*\prime}$ and $y^{*\prime}$ axes, respectively

$$u_A(\xi^{*\prime}, \eta^{*\prime}) = u_{M,CM} - \alpha_{\eta^*}\xi^{*\prime} + \frac{1}{\Lambda^*}\alpha_{\xi^*}\eta^{*\prime} \tag{17}$$

The additional unknown terms in Eq. (17) — $u_{A,CM}$, α_{η^*} , and α_{ξ^*} — can be expressed as a function of dimensionless frequency parameter k^*, dimensionless mass parameter $\mu^* = M_A/(m_A' L_x^{*2})$, dimensionless rotational inertia parameters $\vartheta_{\xi^*} = J_{x^*}/(M_A L_x^{*2})$ and $\vartheta_{\eta^*} = J_{y^*}/(M_A L_x^{*2})$, and the point-force coupling terms γ_i^*according to

$$u_M, C_M = \frac{1}{\mu^* k^{*2}} \sum_{i=1}^{I^*} \gamma_i^* \tag{18}$$

$$\alpha_{\xi^*} = \frac{1}{\mu^* k^{*2} \Lambda^* \vartheta_{\xi^*}} \sum_{i=1}^{I^*} \xi_i^{*\prime} \gamma_i^* \tag{19}$$

$$\alpha_{\eta^*} = \frac{1}{\mu^* k^{*2} \vartheta_{\eta^*}} \sum_{i=1}^{I^*} \eta_i^{*\prime} \gamma_i^* \tag{20}$$

$$u_A(\xi^{*\prime}, \eta^{*\prime}) = \frac{1}{\mu^* k^{*2}} \sum_{i=1}^{I^*} \left(1 + \frac{\xi^{*\prime}\xi_i^{*\prime}}{\vartheta_{\eta^*}} + \frac{\eta^{*\prime}\eta_i^{*\prime}}{\Lambda^{*2}\vartheta_{\xi^*}}\right)\gamma_i^* \tag{21}$$

Since the inertial inclusion is perfectly bonded to the array, its motion will match identically the motion of the plate at each of the I^* colocation points, implying

$$u_A\left({\xi^{*\prime}}_m {\eta^{*\prime}}_m\right) = u^*(\xi_m^* \eta_m^*) \quad \text{for } 1 \le m \le I^* \tag{22}$$

which can be written in matrix form according to

$$-\mathbf{L}^{*T}\mathbf{q}^* + \frac{1}{k^2}\mathbf{G}\boldsymbol{\gamma} = 0 \tag{23}$$

where the matrix $G^* = (g_{mn}^*) \in \mathbb{R}^{I^* \times I^*}$ has entries given by

$$g_{mn}^* = \frac{1}{\mu^*}\left(1 + \frac{\xi^{*\prime}\xi_i^{*\prime}}{\vartheta_\eta^*} + \frac{\eta^{*\prime}\eta_i^{*\prime}}{\Lambda^{*2}\vartheta_{\xi^*}}\right) \tag{24}$$

Combining equations Equations (12) and (23) into a single block matrix, the resulting equations of motion can be expressed as

$$\begin{bmatrix} \boldsymbol{C}^* - k^{*2}\boldsymbol{M}^* & -\boldsymbol{L}^* \\ -\boldsymbol{L}^{*T} & \boldsymbol{G}^*/_{k^{*2}} \end{bmatrix} \begin{bmatrix} \boldsymbol{q}^* \\ \boldsymbol{\gamma}^* \end{bmatrix} = \beta^* \begin{bmatrix} \boldsymbol{b}^* \\ 0 \end{bmatrix} \tag{25}$$

whose homogeneous form can be expressed as the generalized eigenvalue problem given by

$$\mathbf{A}^*\mathbf{x}^* = k^{*2}\mathbf{B}^*\mathbf{x}^* \tag{26}$$

where

$$\mathbf{A}^* = \begin{bmatrix} \boldsymbol{C}^* & -\boldsymbol{L}^* \\ 0 & \boldsymbol{G}^* \end{bmatrix}, \mathbf{B}^* = \begin{bmatrix} \boldsymbol{M}^* & 0 \\ \boldsymbol{L}^{*T} & 0 \end{bmatrix}, \text{ and } \mathbf{x} = \begin{bmatrix} \boldsymbol{x}_q^* \\ \boldsymbol{x}_\gamma^* \end{bmatrix} \tag{27}$$

The solution to this eigenvalue problem is found using standard solvers to identify the first K* eigenvalues (indicating dimensionless modal frequencies) and eigenvectors (indicating coupling forces at collocation points and modal coefficients for eigenfunction weighting coefficients).

The steady-state behavior of the structure under forced vibration can be determined by approximating the solution to Equation (25) as a finite linear combination of the first K* eigenmodes. This approximation is captured in Equation (28)

$$[\ \boldsymbol{q}^{*T}\boldsymbol{\gamma}^{*T}\ ]^T \approx \mathbf{X}^*\mathbf{c}^*(k^*) \tag{28}$$

where $X^* \epsilon\ \mathbb{R}^{(N^*+I^*)\times K^*}$ is a matrix of eigenvectors such that the i^{th} column corresponds to the i^{th} eigenvector of Equation (26) and $c^* = [c_1^*, c_2^*, \ldots, c_{k^*}^*]^T$ is a vector containing modal contribution coefficients. The modal contribution coefficients can be determined by substituting Equation (28) into Equation (25), pre-multiplying by the matrix X^{*T}, taking advantage of the identity $A^*X^* = B^*X^*\Lambda^*$ (where $\Lambda^* \epsilon\ \mathbb{R}^{K^*\times K^*}$ is a diagonal matrix with entries corresponding to the first K* dimensionless eigenfrequencies extracted from Equation (26)), and rearranging to express these coefficients c* as a function of dimensionless frequency k* and according to

$$\boldsymbol{c}^*(k^*) = \beta^*(\Lambda^* - k^{*2}\boldsymbol{I})^{-1}(\boldsymbol{X}^{*T}\boldsymbol{B}^*\boldsymbol{X}^*)^{-1}\boldsymbol{X}^{*T}\begin{bmatrix} \mathbf{b}^* \\ 0 \end{bmatrix} \tag{29}$$

Please cite the article as: WT Edwards and S Nutt **"Transmission Loss and Dynamic Response of Hierarchical Acoustic Metamaterials",** Journal of Vibration and Acoustics (2019) DOI: 10.1115/1.4045789

2.3.2 Modeling Cell Behavior: Membrane-Like Dynamics.

Using an analogous mathematical framework, the individual membrane cells are described according to a model presented by Langfeldt et al. [13]. The rectangular membrane is given in dimensions L_x and L_y, surface mass density m'_M is subject to a uniform tension force per unit length T and is taken to have perfectly fixed edges.

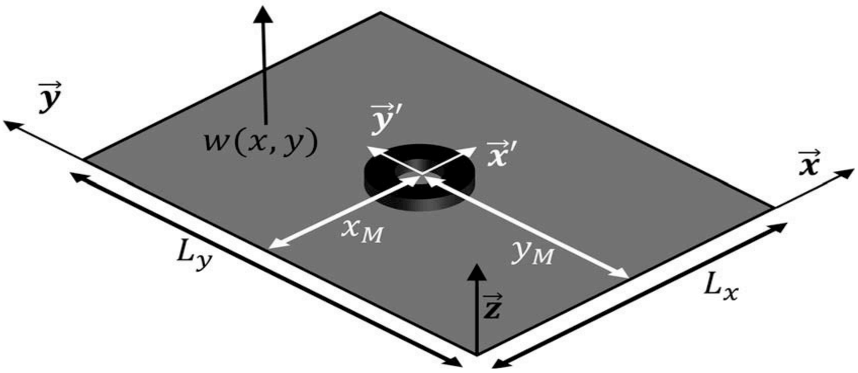

Figure 5. Definition of geometric and mathematical variables for modeling membrane behavior

Bonded in the center of the membrane is an annular inertial inclusion of mass M_M. Geometric parameters and variables are defined in Figure 5, where the origin of the $\{\vec{x}, \vec{y}, \vec{z}\}$ coordinate frame is located at one corner of the membrane with the positive $\vec{x}$- and $\vec{y}$-axes oriented along edges of the membrane. The out of the plane motion of the membrane is given by w(x, y, t) which evolves according to the inhomogeneous wave equation given by Equation (30)

$$m'_M \frac{\partial^2}{\partial t^2} w(x,y,t) - T\nabla^2 w(x,y,t) = P(x,y,t) + f'_M(x,y,t) \tag{30}$$

Equation (30) is normalized using dimensionless parameters analogous to those used in modeling the array. These parameters are given by Equation (5) when the "*" symbol is dropped from each term and the subscript "M" (for membrane) is substituted for the subscript "A" (for array) where appropriate. Modal responses of the membrane cells can then be approximated as a linear combination of N eigenfunctions. The eigenfunctions used to approximate the membrane's modal response are given by $\Phi_n(\xi, \eta) = \Phi_{n_x n_y}(\xi, \eta) = \sin(n_x\pi\xi)\sin(n_y\pi\eta)$ where $n \in \{1, 2, \ldots, N\}$, $n_x \in \{1, 2, \ldots, N_x\}$, $n_y \in \{1, 2, \ldots, N_y\}$, $N = N_x N_y$, and $n = N_y(n_x-1) + n_y$. The matrix equation of motion this produces is analogous to Equation (12)

$$(\mathbf{C} - k^2\mathbf{M})\mathbf{q} = \beta\mathbf{b} + \mathbf{L}\boldsymbol{\gamma} \tag{31}$$

The entries of the stiffness matrix $C = (c_{mn}) \in \mathbb{R}^{N\times N}$, mass matrix $M =(m_{mn}) \in \mathbb{R}^{N\times N}$, forcing vector $b = (b_n) \in \mathbb{R}^{N}$, and coupling matrix $L =(l_{mi}) \in \mathbb{R}^{N\times I}$ have entries given by

$$c_{mn} = \begin{cases} \frac{\Pi^2}{4}(n_x^2 + \Lambda^2\, n_y^2) & for\ m = n \\ 0 & else \end{cases} \tag{32}$$

$$m_{mn} = \begin{cases} \frac{1}{4} & for\ m = n \\ 0 & else \end{cases} \tag{33}$$

$$b_n = \begin{cases} \frac{4}{\Pi^2 n_x n_y} & \text{for } n_x n_y \text{ odd} \\ 0 & \text{else} \end{cases} \tag{34}$$

$$l_{mi} = \sin(m_x\pi\xi_i)\, \sin(m_y\pi\eta_i) \tag{35}$$

The coupling effect between the continuously vibrating membrane and the rigid, bonded mass is approximated by the same point-matching approach as described in Section 2.3.1. A selection of I discrete colocation points, located within (and on the boundary of) the domain of the annular inclusion, was used to approximate continuous-domain coupling. Equations describing the motion of the inertial inclusion on the membrane are given according to Equation (21) when the "*" symbol is dropped from each of the terms and the subscript "M" is substituted for the subscript "A" in uA. Further, the equivalence relation between equations of motion for each body at each of the I colocation points is given in matrix format by Equation (23), and entries to the matrixGare given by Eq. (24)—again, the "*" symbol is dropped from each of the terms in both equations.

The resulting matrix equation of motion describing the vibration of the membrane cell is given by

$$\begin{bmatrix} \boldsymbol{C} - k^2\boldsymbol{M} & -\boldsymbol{L} \\ -\boldsymbol{L}^T & \boldsymbol{G}/_{k^2} \end{bmatrix} \begin{bmatrix} \boldsymbol{q} \\ \boldsymbol{\Upsilon} \end{bmatrix} = \beta \begin{bmatrix} \boldsymbol{b} \\ 0 \end{bmatrix} \quad (36)$$

The homogeneous part of the resulting equation is solved in the same fashion as above: by finding the first K eigenvalues and eigenvectors of

$$\mathbf{Ax} = \mathrm{k}^2\mathbf{Bx} \quad (37)$$

where

$$\mathbf{A} = \begin{bmatrix} \boldsymbol{C} & -\boldsymbol{L} \\ 0 & \boldsymbol{G} \end{bmatrix}, \mathbf{B} = \begin{bmatrix} \boldsymbol{M} & 0 \\ \boldsymbol{L}^T & 0 \end{bmatrix}, \text{ and } \mathbf{x} = \begin{bmatrix} \boldsymbol{x}_q \\ \boldsymbol{x}_\Upsilon \end{bmatrix} \quad (38)$$

These solutions are then used to approximate the inhomogeneous solution, calculating the mode participation factors c in the same method as outlined above according to

$$\mathbf{c}(\mathrm{k}) = \beta(\wedge - k^2\boldsymbol{I})^{-1}(\boldsymbol{X}^T\boldsymbol{B}\boldsymbol{X})^{-1}\boldsymbol{X}^T \begin{bmatrix} \mathbf{b} \\ 0 \end{bmatrix} \quad (39)$$

2.3.3 Transmission Loss: Compound Structure. The dynamic response of each of the two length scales of the array of MAMs is used to estimate the acoustic transmission properties of the system. Transmission efficiencies through both the membrane and the array are each determined under the assumption that the surface-averaged vibration amplitude dominates the sound radiation behavior of the system. This assumption is appropriate for frequencies with acoustic wavelength $\lambda > \sqrt{L_x^{*2} + L_y^{*2}}$ larger than the characteristic length of the array. Because low-frequency performance is of primary interest, this assumption is not particularly restrictive and is discussed more thoroughly below. The surface-averaged vibration amplitude is used to determine the effective mass density of the structure, from which transmission loss can be predicted in accordance with the acoustic mass law. In accordance with Newton's Second law, the effective mass density of the compound structure $\widetilde{m}'_{CE}$ is expressed as

$$\widetilde{m}'_{CE} = \frac{\langle P \rangle}{\langle \ddot{w}_{CE} \rangle} = \frac{\langle P \rangle}{\omega^2 \langle w_{CE} \rangle} \quad (40)$$

where ⟨⟩ indicates the surface average of the quantity it encloses. Because the total summed area of the membranes is roughly equivalent to the area of the array itself, the surface average motion of the compound structure $\langle w_{CE} \rangle$ can be estimated as the sum of the surface average motion of the array and the individual membrane cells: $\langle w_{CE} \rangle = \langle w^* \rangle + \langle w \rangle$. Using the relation in Equation (40), rearranging terms, and making the appropriate substitutions for dimensionless parameters, the effective mass density of the compound structure is given by

$$\tilde{m}'_{CE} = (\tilde{m}'^{-1} + \tilde{m}^{*\prime -1})^{-1} \tag{41}$$

where

$$\tilde{m}^{*\prime} = -\frac{m'_A}{k^{*2}[b^{*T} \;\; 0]X^*c^*} \tag{42}$$

$$\tilde{m}' = -\frac{m'_M}{k^2[b^T \;\; 0]Xc} \tag{43}$$

The acoustic mass law is used to calculate the transmission coefficient t according to

$$\frac{1}{t} = 1 + \frac{i\omega\tilde{m}'_{CE}}{2\rho_0 c_0} \tag{44}$$

where ρ_0 and c_0 are the density and speed of sound of the acoustic fluid through which sound is being transmitted (typically air). In this study, the transmission coefficient of the individual membrane cell, the array, and the compound structure were each determined and compared. Finally, transmission through the compound structure can be calculated according to $TL_0 = -20 \log_{10} |t|$.

In the work presented below, the following geometric parameters and derived quantities were used and held constant when modelling the array, membrane, and compound structures: $L_x^* = L_y^* = 0.241$ m, h = 7.5 × 10^{-3} m, $[x_M^*, y_M^*]$ = [0.1205 m, 0.1085 m], $L_x = L_y = 0.040$ m, $x_M = y_M = 0.020$ m, T = 750 N/m, and $m'_M = 0.0971$ kg/m^2. The numerical parameters used were given by $N_x^* = N_y^* = N_x = N_y = 40$, I* = 44, and I = 16. Simulations were conducted for

Please cite the article as: WT Edwards and S Nutt **"Transmission Loss and Dynamic Response of Hierarchical Acoustic Metamaterials",** Journal of Vibration and Acoustics (2019) DOI: 10.1115/1.4045789

combinations of $M_A = \{0, 2.5, 10.3, 20.5\} \times 10^{-3}$ kg and $M_M = \{0, 1.6, 3.2\} \times 10^{-4}$ kg using the appropriate corresponding values of J_{x^*}, J_{y^*}, J_x, and J_y given inclusion geometry.

The areal mass and flexural rigidity of the homogenized array (with no masses bonded to individual membrane cells) were estimated according to m'_A = 1.16 kg/m^2 and T* = 30.77N/m^2. The method for estimating the areal mass of the array was measuring the mass of the array, adhesive, and membrane after assembly (but prior to the placement of individual masses on each membrane cell), subtracting the mass of the edge regions of the array (which are clamped in the test fixture during transmission loss measurement), and dividing the remaining mass by the area of the test window (0.05801 m^2). The mass of the array, adhesive, and bonded membrane was measured to be 0.128 kg, the mass of the array edges clamped in the test fixture were theoretically calculated to be 0.0608 kg, and the resultant areal mass of the homogenized array was determined to be m'_A = 1.16 kg/m^2. When individual membrane cells had masses bonded to them, the areal mass of the homogenized array was increased appropriately. For example, when 0.16 g masses are added to each of the 36 individual membrane cells, this mass is assumed to be distributed uniformly, and the areal mass of the homogenized array is increased to m'_A = 1.26 kg/m^2 to account for this additional inertia. The flexural rigidity of the homogenized array was estimated fixing the areal weight of the homogenized array in the manner previously described, then fitting a value to T* such that the analytical model predictions match experimental data for the fourth eigenfrequency of the homogenized array vibration. This frequency was measured to be approximately 1.8 kHz for the array when 0.16 g masses were attached to individual membrane cells and no mass was attached to the array (m'_A = 1.26 kg/m^2, M_A = 0). The resultant homogenized flexural rigidity of the array used for modeling was estimated to be T* = 30.77N/m^2.

3. RESULTS AND DISCUSSION

The transmission loss was measured and analytically predicted through 12 different configurations of the MAM array structure. The results demonstrated a complex interaction between the two length scales, showed that new transmission properties—present for neither length scale independently—can be achieved in the compound structure, and established the importance of considering this interaction when scaling MAM structures. In this section, we first present transmission loss results characteristic of the hierarchical metamaterial structure fabricated for this study and explain the vibroacoustic behavior responsible for features of interest. Subsequently, we demonstrate the effect of varying the mass of the inertial inclusions bonded to both the array and the individual membrane cells. Finally, we discuss the limitations of the modelling approach presented in Sec. 2.3 and indicate possible future extensions or improvements in the model.

3.1 Hierarchical Acoustic Metamaterial: Characteristic Performance. The experimentally measured transmission loss through the array of 36 MAM cells is plotted in Figure 6 for the case of $M_A = 2.5 \times 10^{-3}$ kg and $M_M = 1.6 \times 10^{-4}$ kg. Experimental data in this figure are

Please cite the article as: WT Edwards and S Nutt **"Transmission Loss and Dynamic Response of Hierarchical Acoustic Metamaterials",** Journal of Vibration and Acoustics (2019) DOI: 10.1115/1.4045789

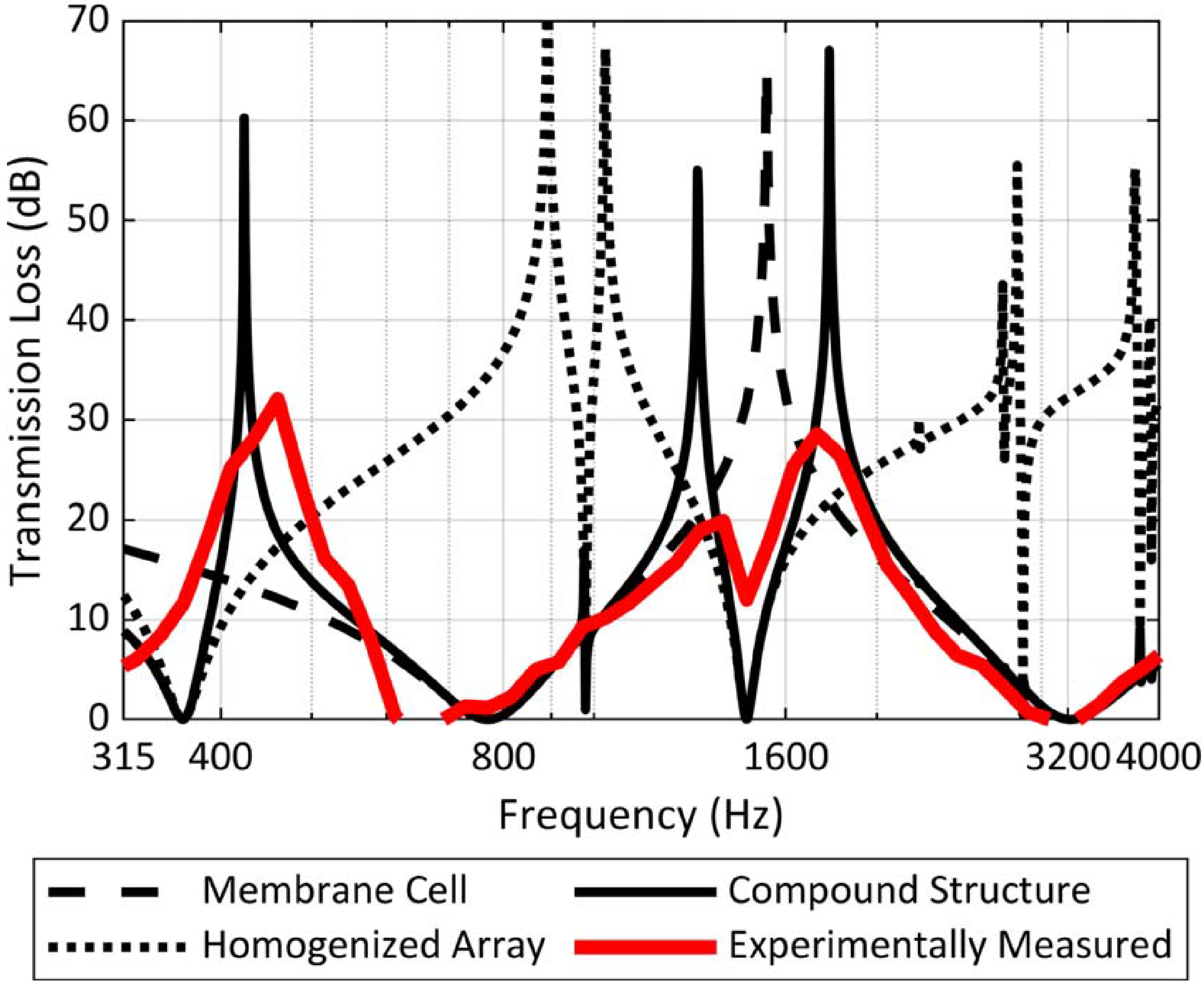

Figure 6. Characteristic transmission loss performance of hierarchical acoustic metamaterial

compared against analytical predictions for transmission loss through the individual membrane cells, the homogenized array, and the compound structure. It is apparent that the transmission loss properties of the compound structure arise directly from the behavior of, and interaction between, each length scale of the structure. Previous work has demonstrated that the low-frequency propagation of acoustic energy through membrane- and plate-type acoustic metamaterials is determined by the modal responses of such structures. Similarly, it is apparent that the modal responses of each length scale of the hierarchical metamaterial contribute to the transmission properties of the structure. The modal contributions responsible for each local minima and maxima are explained. When interpreting Figure 6, it is worth noting that estimates for the performance of neither length scale individually (the membrane cell scale or the homogenized array scale) is anticipated to match the estimates produced by the compound model or experimental data across the whole frequency range. Features such as minima in estimates of the performance of each length scale are apparent in the compound model over narrow frequency ranges, but (appropriately) when transmission loss is non-zero for both length scales, a more complex interaction between the two levels of hierarchy occurs. Rather than to achieve good matching with the compound model or experimental data, Figure 6 includes estimates of the performance of each length scale to explain the origin of transmission loss maxima and minima apparent in the compound model prediction and experimental measurements.

Four experimentally measured transmission loss local minima can be seen in Figure 6 at frequencies of 315 Hz, 765 Hz, 1455 Hz, and 3200 Hz. At each of these frequencies, the transmission loss of the compound structure is dominated by the behavior of one of its two constituent length scales. That is, the behavior of the homogenized array dictates the transmission loss behavior at 315 Hz and 1455 Hz, while the behavior of the individual MAM cells dictates the behavior at 765 Hz and 3200 Hz. At each of these frequencies, the compound structure is nearly transparent to acoustic propagation, and the admittance of nearly all-acoustic energy through the structure is explained by the excitation of a mode (either modes of the homogenized array or modes of the membrane cells) characterized by non-zero average surface motion during oscillation.

The first transmission loss minimum in Fig. 7, near 315 Hz, corresponds to activation of the first fundamental mode of the homogenized array. While analytic techniques predicted this mode to occur at approximately 360 Hz, experimental data indicated that the first resonance

Please cite the article as: WT Edwards and S Nutt **"Transmission Loss and Dynamic Response of Hierarchical Acoustic Metamaterials",** Journal of Vibration and Acoustics (2019) DOI: 10.1115/1.4045789

of the array occurs near the transmission loss minimum at 315 Hz. Acoustic energy is efficiently transmitted through the hierarchical acoustic metamaterial at this frequency—

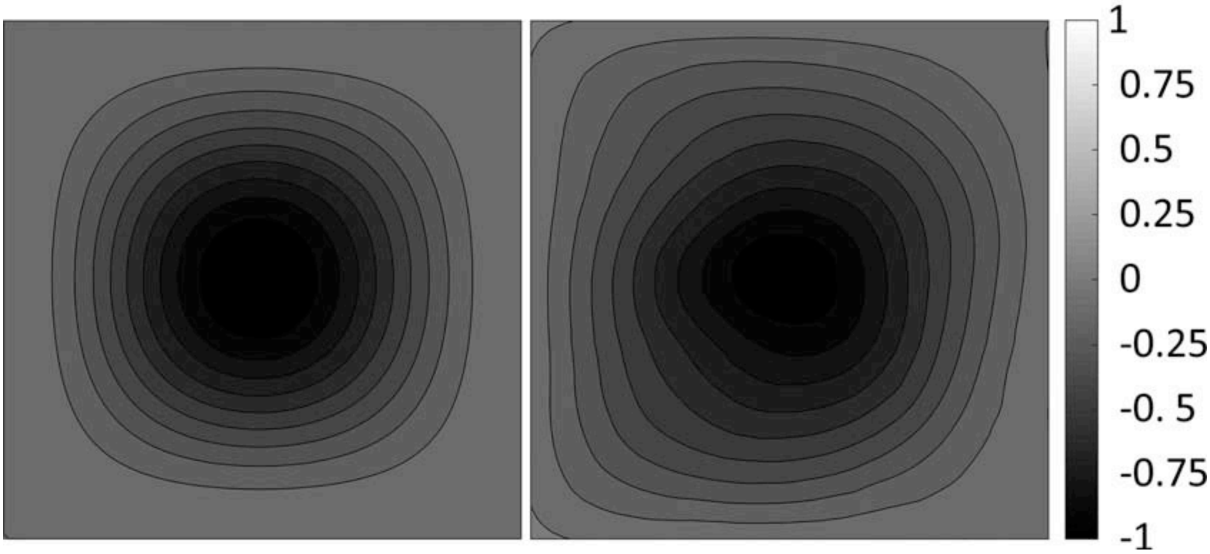

Fig. 7 First modal response of homogenized array as predicted analytically (left) and measured experimentally (right)

resulting in a transmission loss of nearly zero—because the surface-averaged motion of the array oscillating in this mode is non-zero. Further, because the effective mass density of the homogenized array ($\widetilde{m}^{*\prime}$) is nearly zero at the first fundamental mode of array vibration, the term contributed by the array to Equation (41) far outweighs the term contributed by the membrane cell-level behavior. This explains why array-level behavior dominates the performance of the compound structure near the first transmission loss minimum.

The analytically predicted (left) and experimentally measured (right) modal responses of the array oscillating in its first mode of vibration are pictured in Figure 7. Experimental mode shape plots were produced by fitting a surface to the 85 vibrometer measurements using a locally weighted scatterplot smoothing algorithm, normalizing out of plane deformation, and generating contour lines and shading to indicate the magnitude and direction of out of plane array deformation. In Figure 7, as for all figures showing the modal response of the membrane or array, regions of deformation below the neutral plane appears darker than regions of deformation above the neutral plane. A normalized deformation value of negative one corresponds to black coloration and normalized deformation of positive one corresponding to white coloration. The similarity of the analytical and experimental modal responses pictured in Figure 7 indicates the efficacy of the modeling approach presented herein. Discrepancies between the two modal response shapes can likely be attributed to noise in the laser vibrometry data and imperfectly clamped array edges.

The second transmission loss minimum corresponds to the activation of the first mode of the individual MAM cells. Analytic and experiment data agree that this mode is located at approximately 765 Hz. The shape of membrane deformation under excitation at this frequency is analogous to the first mode of the vibrating array (see Figure 6) and similarly produces a non-zero surface-averaged displacement during oscillation, resulting in efficient transmission through the structure, and dominating performance over array-scale behavior at this frequency.

From Figure 6, it is apparent that the third analytically predicted and experimentally measured transmission loss minimum can be attributed to the dynamics of the array. Experimental and theoretical results agree that the fourth fundamental mode of array vibration is located at approximately 1455 Hz. Activation of this mode dominates transmission loss characteristics of the compound structure at this frequency. Because the surface-averaged deformation of the array is significant at this frequency, acoustic energy is efficiently transmitted, resulting in a transmission loss minimum. The analytically predicted and experimentally measured mode shapes for this frequency achieve excellent agreement and are shown in Figure 8. Unlike with the first transmission loss minimum of the compound structure, the experimental and analytical data indicate non-zero transmission loss at this frequency despite the analytic model of the homogenized array indicating that zero transmission loss should be achieved. Indeed, experimental measurements indicate that transmission loss of no less than 12 dB is in the vicinity of this frequency. This discrepancy can likely be attributed to the frequency band averaging performed during experimental data collection and compound model result processing. The effect of averaging transmission loss data over a 1/8th octave band

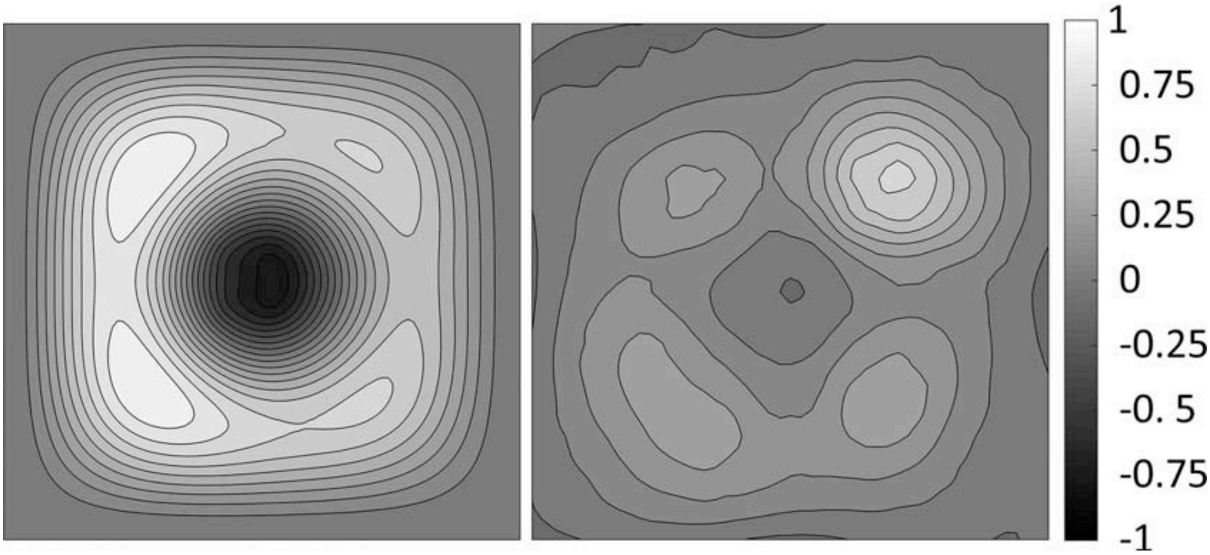

Figure 8. Second quasi-symmetric modal response of array as predicted analytically (left) and measured experimentally (right)

is exacerbated by the relatively narrow frequency range at which this mode of the array achieves large amplitude vibration.

The fourth experimental transmission loss minimum in Figure 6 is correlated with the fourth modal response (second symmetric response) of the individual membrane cells. Experimental and analytical results locate this mode at approximately 3200 Hz. An analytical prediction of the mode shape at this frequency is shown in Figure 9. The apparent non-zero surface-averaged displacement seen in this figure explains the efficiency of acoustic transmission through the structure at this frequency.

At each of the minima discussed, the transmission properties of the structure are dominated by the vibratory behavior of a single length scale, where resonance results in large volumetric displacement across the neutral plane of the structure. Transmission loss maxima,

Please cite the article as: WT Edwards and S Nutt **"Transmission Loss and Dynamic Response of Hierarchical Acoustic Metamaterials",** Journal of Vibration and Acoustics (2019) DOI: 10.1115/1.4045789

however, are not dominated by the behavior of either length scale individually, and instead, require the sum of volumetric displacements for each length scale to be zero. For example, modeling data describing the compound structure indicate the first transmission loss peak in Figure 6 occurs at approximately 430 Hz where the structure achieves a transmission loss of 35 dB. There is no local maximum for either the array or membrane length scales at this frequency, however, and the transmission loss predicted at each length scale is found to be 14 dB and 13 dB for the array and membrane, respectively. The increased transmission loss when compared against either individual length scale can be attributed to the phase difference between the motion of the array and the membrane cells. At this frequency, the motion of the array lags the acoustic excitation signal by about pi radians, while the motion of the individual membrane cells is approximately in phase with the excitation signal, resulting in near-zero net displacement during oscillation, and efficient rejection of acoustic energy.

Like the first transmission loss maximum, the second and third maxima in the analytical compound structure predictions are located at frequencies for which the surface-averaged

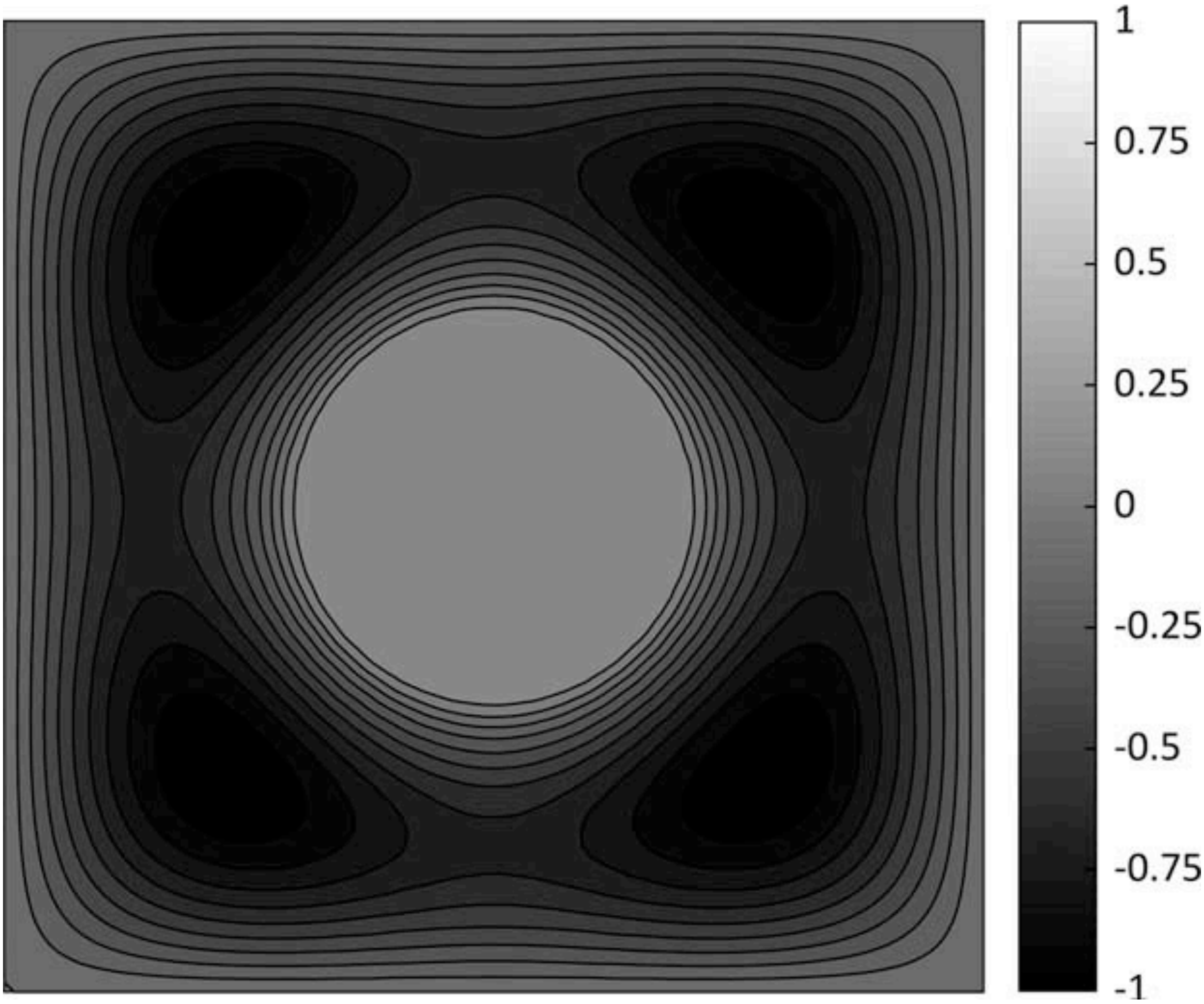

Figure 9. Analytical prediction of second symmetric mode shape in individual membrane cells

displacement of the homogenized array is predicted to be equal and opposite to the surface-averaged displacement of the individual membrane cells. Such frequencies are located at or immediately adjacent to frequencies at which the transmission loss curves of the two length scales cross. The second transmission loss maximum of the compound structure is predicted to be at 1275 Hz, near the frequency where the transmission loss curves of the homogenized array and membrane cell cross over at 20.3 dB. The third transmission loss maximum is similarly located at such a crossover point at 1775 Hz. These analytically predicted transmission loss maxima correspond reasonably well with experimental data, indicating the effectiveness of the modeling approach presented in this paper.

Please cite the article as: WT Edwards and S Nutt **"Transmission Loss and Dynamic Response of Hierarchical Acoustic Metamaterials",** Journal of Vibration and Acoustics (2019) DOI: 10.1115/1.4045789

3.2 Parametric Effect of Inertial Inclusions. By varying the size of the inertial inclusions incorporated into each length scale of the hierarchical acoustic metamaterial, the frequencies at which characteristic transmission loss peaks and dips can be shifted. Figure 10 shows measured and predicted transmission properties through the structure studied for $M_M = 0$ kg and various values of M_A. As M_A increases, the frequency at which the first transmission loss dip occurs, corresponding to the first symmetric eigenmode of the array, decreases. Similarly, the frequency of the first transmission loss peak is also shifted to a lower frequency range. Note, however, that features on the curve above approximately 800 Hz are unaffected by changes in MA. This is because the dynamics of the membrane dominate the transmission performance of the structure above this frequency, resonating with a large amplitude over a wide frequency band. Further, the lack of inertial inclusions on the individual membrane cells results in a second symmetric mode that is unfavorable for sound rejection.

The parametric influence of M_A can be further characterized as shown in Figure 11, where the size of the mass on the membrane cells is $M_M = 1.6 \times 10^{-4}$ kg. In this figure, the influence of the second symmetric mode of the array becomes clearer. The eigenfrequencies associated with this mode for each case of increasing M_A are given as 1791 Hz, 1600 Hz, 1377 Hz, and 1297 Hz, respectively. For each case, the transmission efficiency of the structure is enhanced in the neighborhood of this frequency, and transmission loss is reduced. This phenomenon is largely responsible for the

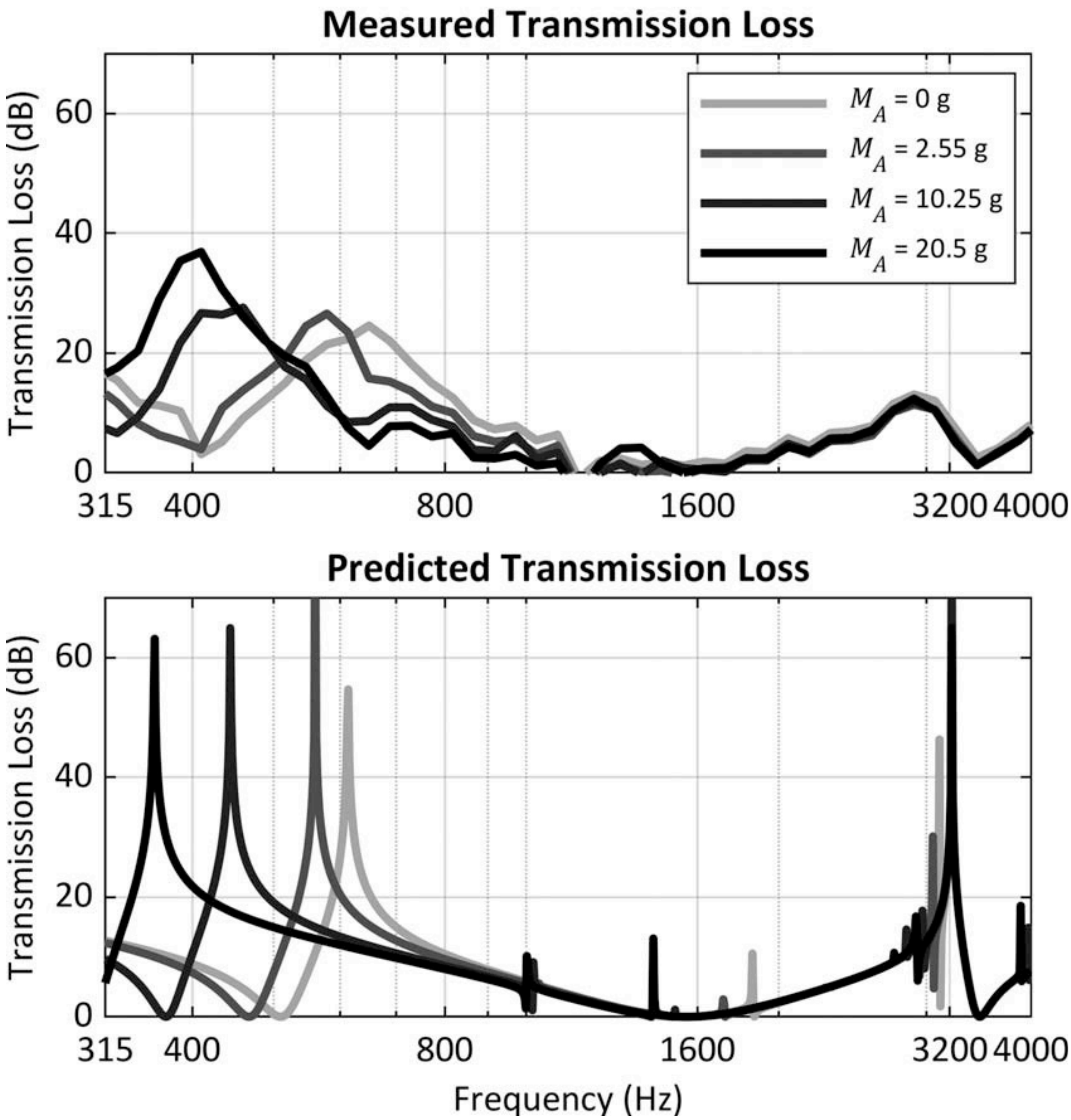

Figure 10. Parametric effects of MA on transmission properties for $M_M = 0$ g

Please cite the article as: WT Edwards and S Nutt **"Transmission Loss and Dynamic Response of Hierarchical Acoustic Metamaterials",** Journal of Vibration and Acoustics (2019) DOI: 10.1115/1.4045789

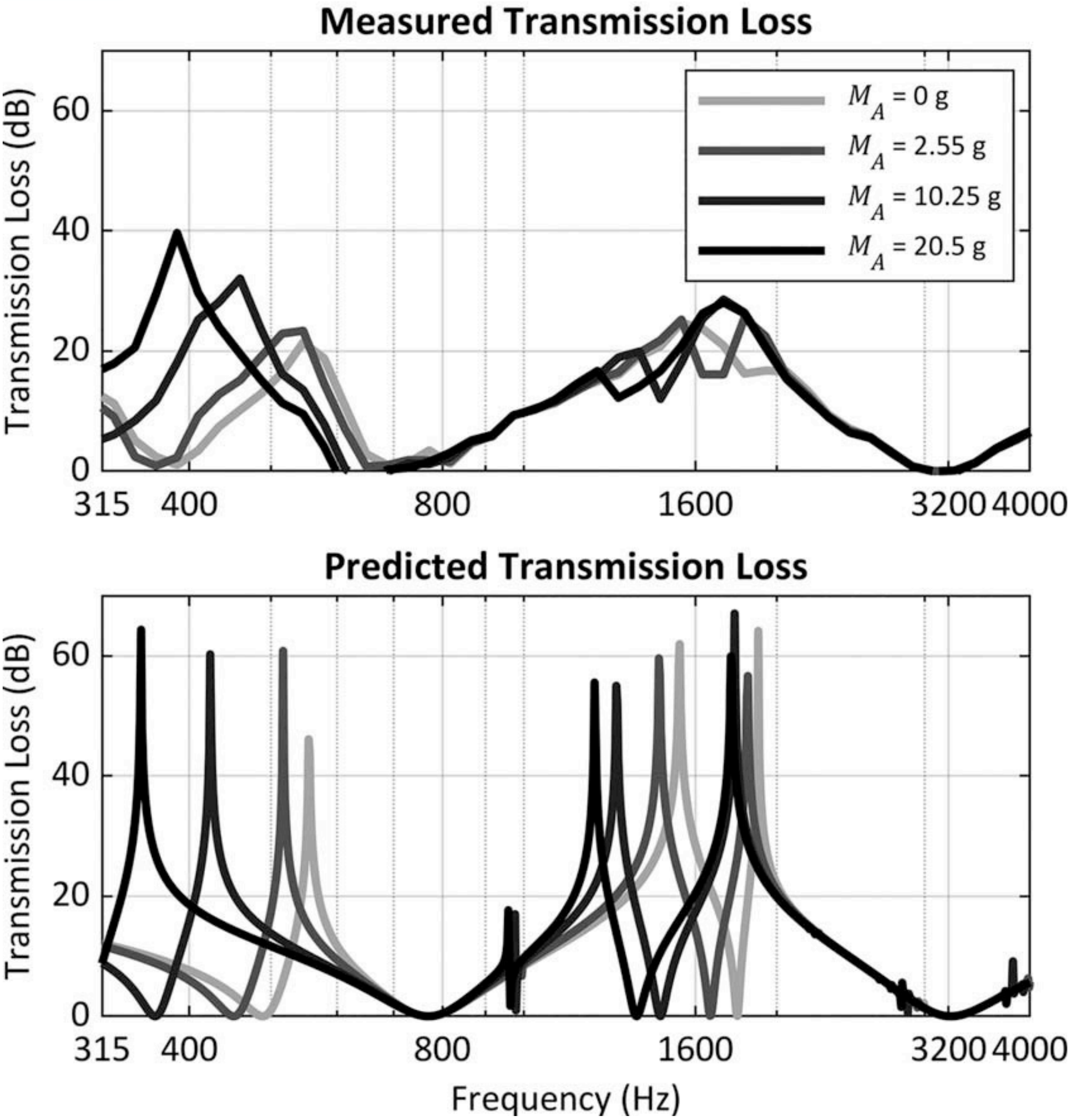

Figure 11. Parametric effects of MA on transmission properties for M_M=1.6 × 10−4 kg

decay of transmission loss performance that is associated with the scaling of MAM structures. The figure demonstrates the importance of considering the dynamics of the array, as the modal responses can provide efficient parallel transmission paths that are highly efficient in some frequency ranges.

3.3 Accuracy and Extensions to the Modeling Approach.

Readers may notice several differences between the analytical predictions and experimental data presented in Figures 10 and 11. Some of these differences can be attributed to the averaging necessary for the collection of experimental transmission loss data that are not present in the analytical predictions. Because experimental data are averaged over a 1/8th octave band around each sampling frequency, the magnitude of the transmission loss maxima and minima measured are significantly less extreme than those estimated by the analytical tool. Averaging of the experimental data is largely responsible for the difference between model predictions and measurements in Figure 11 in the range of 1–2 kHz. When analytical data are subjected to 1/8th octave band averaging over this range and sampled at the same frequencies as experimental data, the minimum forecast transmission loss increases from 0 dB to 8–14 dB (depending on array mass loading condition), and the maximum forecast transmission loss data decreases from infinite to 30–45 dB. Averaging of the analytical data also entirely obfuscates the transmission loss maxima and minima analytically predicted to occur just below 1 kHz in Fig. 11. Indeed, such local extrema are not seen in the measured transmission loss data. Overall, averaging the estimated transmission loss results in a much closer match with experimental measurements, and the effect of such averaging is not always intuitive due to the logarithmic nature of transmission loss data and frequency sampling.

Beyond the difference between averaged and unaveraged transmission loss data, the experimental and analytical results likely deviate from one another due to variability in membrane tension and mass size and location within each membrane cell. While each MAM cell in the array was intended to be identical, imperfections in the machining of the array, the thickness of the membrane, adhesion of the bond between the two, and location and size of the mass placed on each membrane cell no doubt resulted in a distribution of similarly tuned membrane cells. The effect of this on the transmission loss through the structure would serve

Please cite the article as: WT Edwards and S Nutt **"Transmission Loss and Dynamic Response of Hierarchical Acoustic Metamaterials",** Journal of Vibration and Acoustics (2019) DOI: 10.1115/1.4045789

to further reduce the extremity of the maxima and minima predicted analytically throughout the frequency range of interest. Such a difference in the tuning of individual membrane cells is likely responsible for differences in the shape of the experimental and analytical transmission loss profiles near the first maximum in Figures 10 and 11. At this transmission loss maximum, the volume velocity of the sum of membrane cells is approximately equal to and opposite of the volume velocity of the array structure. This results in inefficient transmission through the metamaterial, yielding high transmission loss. Analytical tools assume that all membrane cells are oscillating with identical shape and that they are perfectly phase matched. The inherent variability in the manufacturing of the array of MAMs, however, prevents such synchronistic motion from being physically realized. The effect of this distribution of frequency responses in individual membrane cells is such that the measured transmission loss maximum is broader but of reduced amplitude around this frequency when compared against analytical estimates.

Some of the differences between the estimated and measured transmission loss data are due to the limitations of approximating the membrane array as a homogenized plate rather than a true array. Data indicate that this assumption is a useful first-order approximation, but authors acknowledge that the eigenfrequencies and mode shapes of a grid do not match identically with those of an equivalent isotropic, homogeneous plate. Further, the nature of the homogenization scheme used, whereby the flexural rigidity was determined using the measured response of the array near 1.6 kHz, is such that the analytical estimate of behavior is anticipated to be accurate near this frequency, but accumulate error when moving toward significantly higher or lower regimes. Indeed, this is demonstrated in Figures 10 and 11 where analytical and experimental data deviate most significantly at the lowest frequencies considered. The authors anticipate that the accuracy of the model could be improved if the array length scale of the hierarchical structure was modeled as a grid rather than a homogenized plate.

One additional way that the accuracy of the model could be improved would be to include the effect of motion coupling between the array and membrane cell scales. Incorporation of such a coupling term would require simultaneous solving of the membrane and array length-scale behaviors. The impact of considering this coupling would be most significant in the low-frequency range where array deformation is the largest. In high-frequency ranges where the amplitude of array deformation is smaller, the assumption of zero-displacement membrane cell edges is better satisfied, and the consideration of motion coupling would have a smaller impact.

It is worth noting here that while this modeling approach was uniquely developed to describe hierarchical MAMs, and it cannot be used to study different types of hierarchical metamaterials, the model can be extended to capture the effect of additional degrees of hierarchy in these structures. If, for example, each membrane cell comprised an array of MAMs, then modeling this additional length scale could be done in a manner similar to how the membrane and array length-scale behavior was estimated and combined into the compound model in the same manner as described in Section 2.3.3.

4. CONCLUSIONS

The acoustic behavior of deployment-scale arrays of locally resonant MAM structures was investigated. Vibroacoustic behavior responsible for the decay of transmission loss properties typically associated transitioning from a single MAM cell to an array of cells was explained using experimental and analytical results. A novel hierarchical design approach was proposed, considering both the individual membrane cells and the array of membranes as independent, locally resonant acoustic metamaterials that can each be tuned by varying stiffness and mass parameters. A theoretical approach for predicting transmission loss through such structures was presented and validated against experimental data. Results indicated the importance of considering dynamic properties of the frame used to mount individual MAM cells and demonstrated that hierarchical design can be an effective tool to maximize transmission loss performance in regimes of interest.

The practical significance of this work is that it provides acousticians and materials scientists with an effective strategy for maximizing the performance of MAM structures. The analytical tools presented herein grant designers a toolbox that can be used prior to costly sample fabrication and testing. Engineers can confirm and ensure favorable interaction between membrane- and array-scale dynamics during the design process. The primary limitation of the technique presented herein, however, is that the required addition of mass to the membrane array compromises the weight efficiency of the structure. Further, as the size of MAM arrays increases, assumptions about the phenomena dominating acoustic transmission through the structure begin to break down. As a consequence, larger MAM array structures may face inherent limitations to the frequencies in which they can operate or the efficiency they can achieve.

References

[1] Wang, T., Sokolinsky, V. S., Rajaram, S., and Nutt, S. R., 2005, "Assessment of Sandwich Models for the Prediction of Sound Transmission Loss in Unidirectional Sandwich Panels," Appl. Acoust., 66(3), pp. 245–262.
[2] Yang, Z., Mei, J., Yang, M., Chan, N. H., and Sheng, P., 2008, "Membrane-Type Acoustic Metamaterial With Negative Dynamic Mass," Phys. Rev. Lett., 101(20), p. 204301.
[3] Zhang, Y., Wen, J., Xiao, Y., Wen, X., and Wang, J., 2012, "Theoretical Investigation of the Sound Attenuation of Membrane-Type Acoustic Metamaterials," Phys. Lett. A, 376(17), pp. 1489–1494.
[4] Naify, C. J., Chang, C. M., McKnight, G., and Nutt, S., 2010, "Transmission Loss and Dynamic Response of Membrane-Type Locally Resonant Acoustic Metamaterials," J. Appl. Phys., 108(11), p. 114905.
[5] Naify, C. J., Chang, C., McKnight, G., and Nutt, S., 2011, "Transmission Loss of Membrane-Type Acoustic Metamaterials With Coaxial Ring Masses," J. Appl. Phys., 110(12), p. 124903.
[6] Lu, Z., Cui, Y., and Debiasi, M., 2016, "Active Membrane-Based Silencer and Its Acoustic Characteristics," Appl. Acoust., 111, pp. 39–48.
[7] Ma, G., Fan, X., Sheng, P., and Fink, M., 2018, "Shaping Reverberating Sound Fields With an Actively Tunable Metasurface," Proc. Natl. Acad. Sci. U. S. A., 115(26), pp. 6638–6643.

[8] Chen, S., Fan, Y., Fu, Q., Wu, H., Jin, Y., Zheng, J., and Zhang, F., 2018, "A Review of Tunable Acoustic Metamaterials," Appl. Sci., 8(9), p. 1480.
[9] Huang, L., 1999, "A Theoretical Study of Duct Noise Control by Flexible Panels," J. Acoust. Soc. Am., 106(4), pp. 1801–1809.
[10] Du, J., Liu, Y., and Zhang, Y., 2016, "Influence of Boundary Restraint on Sound Attenuation Performance of a Duct-Membrane Silencer," Appl. Acoust., 105, pp. 156–163.
[11] Liu, Y., and Du, J., 2017, "Coupling Effects of Boundary Restraining Stiffness and Tension Force on Sound Attenuation of a Cavity-Backed Membrane Duct Silencer," Appl. Acoust., 117, pp. 150–159.
[12] Chen, Y., Huang, G., Zhou, X., Hu, G., and Sun, C., 2014, "Analytical Coupled Vibroacoustic Modeling of Membrane-Type Acoustic Metamaterials: Membrane Model," J. Acoust. Soc. Am., 136(3), pp. 969–979.
[13] Langfeldt, F., Gleine, W., and von Estorff, O., 2015, "Analytical Model for Low-Frequency Transmission Loss Calculation of Membranes Loaded With Arbitrarily Shaped Masses," J. Sound Vib., 349, pp. 315–329.
[14] Chen, Y., Huang, G., Zhou, X., Hu, G., and Sun, C.-T., 2014, "Analytical Coupled Vibroacoustic Modeling of Membrane-Type Acoustic Metamaterials: Plate Model," J. Acoust. Soc. Am., 136(6), pp. 2926–2934.
[15] Edwards, W. T., Chang, C.-M., McKnight, G., and Nutt, S. R., 2019, "Analytical Model for Low-Frequency Transmission Loss Calculation of Zero-Prestressed Plates With Arbitrary Mass Loading," ASME J. Vib. Acoust., 141(4), p. 041001.
[16] Naify, C. J., Chang, C. M., McKnight, G., Scheulen, F., and Nutt, S., 2011, "Membrane-Type Metamaterials: Transmission Loss of Multi-Celled Arrays," J. Appl. Phys., 109(10) p. 104902.
[17] Naify, C. J., Chang, C.-M., McKnight, G., and Nutt, S. R., 2012, "Scaling of Membrane-Type Locally Resonant Acoustic Metamaterial Arrays," J. Acoust. Soc. Am., 132(4), pp. 2784–2792.
[18] Langfeldt, F., Gleine, W., and von Estorff, O., 2018, "An Efficient Analytical Model for Baffled, Multi-Celled Membrane-Type Acoustic Metamaterial Panels," J. Sound Vib., 417, pp. 359–375.
[19] Langfeldt, F., and Gleine, W., 2019, "Membrane- and Plate-Type Acoustic Metamaterials With Elastic Unit Cell Edges," J. Sound Vib., 453, pp. 65–86.
[20] Imbeni, V., Kruzic, J. J., Marshall, G. W., Marshall, S. J., and Ritchie, R. O., 2005, "The Dentin–Enamel Junction and the Fracture of Human Teeth," Nat. Mater., 4(3), pp. 229–232.
[21] Cranford, S. W., Tarakanova, A., Pugno, N. M., and Buehler, M. J., 2012, "Nonlinear Material Behaviour of Spider Silk Yields Robust Webs," Nature, 482(7383), pp. 72–76.
[22] Zhang, P., and To, A. C., 2013, "Broadband Wave Filtering of Bioinspired Hierarchical Phononic Crystal," Appl. Phys. Lett., 102(12), p. 121910.
[23] Miniaci, M., Krushynska, A., Gliozzi, A. S., Kherraz, N., Bosia, F., and Pugno, N. M., 2018, "Design and Fabrication of Bioinspired Hierarchical Dissipative Elastic Metamaterials," Phys. Rev. Appl., 10(2), p. 024012.
[24] Lee, K. Y., and Jeon, W., 2018, "Hierarchically Structured Metamaterials With Simultaneously Negative Mass Density and Young's Modulus by Using Dynamic Homogenization," J. Appl. Phys., 124(17), p. 175103.
[25] Xu, X., Barnhart, M. V., Li, X., Chen, Y., and Huang, G., 2019, "Tailoring Vibration Suppression Bands With Hierarchical Metamaterials Containing Local Resonators," J. Sound Vib., 442, pp. 237–248.

[26] ASTM, 2016, “ASTM E2249-02(2016) Standard Test Method for Laboratory Measurement of Airborne Transmission Loss of Building Partitions and Elements Using Sound Intensity,” pp. 1–15.
[27] Rajaram, S., Wang, T., and Nutt, S., 2009, “Small-Scale Transmission Loss Facility for Flat Lightweight Panels,” Noise Control Eng. J., 57(5), pp. 536–542.